LANGMUIR

Enhanced Intraliposomal Metallic Nanoparticle Payload Capacity Using Microfluidic-Assisted Self-Assembly

Zahraa S. Al-Ahmady,[†,‡,§] Roberto Donno,[§,∥] Arianna Gennari,[§,∥] Eric Prestat,[⊥,#] Roberto Marotta,[¶] Aleksandr Mironov,[∇] Leon Newman,[†] M. Jayne Lawrence,[§] Nicola Tirelli,[*,§,∥] Marianne Ashford,[*,○] and Kostas Kostarelos[*,†,§]

[†]Nanomedicine Lab, Division of Pharmacy and Optometry, Faculty of Biology, Medicine and Health, University of Manchester, Av Hill Building, Manchester M13 9PT, U.K.

[‡]Pharmacology Department, School of Science and Technology, Nottingham Trent University, Nottingham NG11 8NS, U.K.

[§]North West Centre of Advanced Drug Delivery (NoWCADD), Division of Pharmacy & Optometry, School of Health Sciences, Faculty of Biology, Medicine and Health, University of Manchester, Stopford Building, Manchester, M13 9PT, U.K.

[∥]Laboratory of Polymers and Biomaterials, Fondazione Istituto Italiano di Tecnologia, 16163, Genova, Italy

[⊥]School of Materials and [∇]Electron Microscopy Core Facility, Faculty of Life Sciences, University of Manchester, Manchester M13 9PL, U.K.

[#]SuperSTEM Laboratory, SciTech Daresbury Campus, Keckwick Lane, Warrington WA4 4AD, U.K.

[¶]Electron Microscopy Laboratory, Fondazione Istituto Italiano di Tecnologia, 16163 Genova, Italy

[○]Advanced Drug Delivery Pharmaceutical Sciences, IMED Biotech Unit, AstraZeneca, Macclesfield SK10 2NA, U.K.

S *Supporting Information*

ABSTRACT: Hybrids composed of liposomes (L) and metallic nanoparticles (NPs) hold great potential for imaging and drug delivery purposes. However, the efficient incorporation of metallic NPs into liposomes using conventional methodologies has so far proved to be challenging. In this study, we report the fabrication of hybrids of liposomes and hydrophobic gold NPs of size 2−4 nm (Au) using a microfluidic-assisted self-assembly process. The incorporation of increasing amounts of AuNPs into liposomes was examined using microfluidics and compared to L−AuNP hybrids prepared by the reverse-phase evaporation method. Our microfluidics strategy produced L−AuNP hybrids with a homogeneous size distribution, a smaller polydispersity index, and a threefold increase in loading efficiency when compared to those hybrids prepared using the reverse-phase method of production. Quantification of the loading efficiency was determined by ultraviolet spectroscopy, inductively coupled plasma mass spectroscopy, and centrifugal field flow fractionation, and qualitative validation was confirmed by transmission electron microscopy. The higher loading of gold NPs into the liposomes achieved using microfluidics produced a slightly thicker and more rigid bilayer as determined with small-angle neutron scattering. These observations were confirmed using fluorescent anisotropy and atomic force microscopy. Structural characterization of the liposomal−NP hybrids with cryo-electron microscopy revealed the coexistence of membrane-embedded and interdigitated NP-rich domains, suggesting AuNP incorporation through hydrophobic interactions. The microfluidic technique that we describe in this study allows for the automated production of monodisperse liposomal−NP hybrids with high loading capacity, highlighting the utility of microfluidics to improve the payload of metallic NPs within liposomes, thereby enhancing their application for imaging and drug delivery.
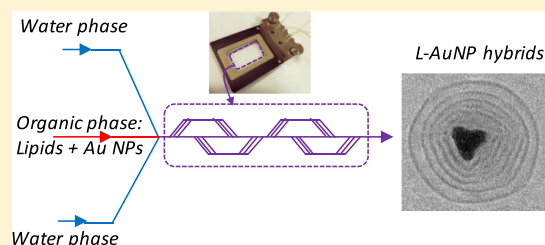
INTRODUCTION

Since their discovery in 1965, liposomes have been widely investigated for various therapeutic and imaging applications and are approved for the treatment of several clinical conditions, in particular for cancer and inflammatory conditions.[1,2] Liposomes are formed by self-assembly of phospholipid molecules into vesicles that can effectively encapsulate hydrophilic drugs in their aqueous core[3,4] and/or incorporate compounds into their lipid membrane.[4−6] Other advantages that liposomes offer include biocompatibility,

biodegradability, modification of blood circulation time and thereby the pharmacokinetic profile of encapsulated drugs mainly through surface modification with PEGylated lipids (i.e., Stealth liposomes).[7] As a consequence of these properties, it is possible to achieve the selective (passive) delivery of liposomes through malformed blood vessels at the disease site

(e.g., into a tumor) while at the same time ensuring minimum accumulation into healthy tissues;[8,9] in this manner, the safety profile of liposomally encapsulated drugs, such as doxorubicin, can be significantly improved.

In addition to the development of liposomes for therapeutic purposes, the engineering of liposomal—metallic nanoparticle (NP) hybrids has also attracted considerable interest for imaging, photothermal, and theranostic (i.e., the combining of imaging/diagnosis and therapy in one delivery system) applications. One example of the benefits of using gold NPs (AuNPs) for imaging and photothermal applications is their surface plasmon resonance properties.[10] Specifically, AuNPs can absorb certain wavelengths of light, resulting in the oscillation of surface electrons and subsequently producing a local heating effect. The intensity and duration of this effect can be altered by modifying the intensity and duration of the laser beam applied, as well as the concentration of AuNPs used.[11] Incorporating AuNPs into liposomes can improve their colloid stability as well as their biological performance.[10,12−20] Indeed, it is well established that stimuli-responsive liposomes can facilitate the site-specific release of the entrapped material in response to external light.[21,22]

There are different methods of L−AuNP hybrid fabrication that have been reported by ourselves and others.[14,23] These can be categorized into three depending on the location of metallic NPs relative to the liposomal membrane, namely, (a) the incorporation of small (<5 nm) hydrophobic NPs into the lipid membrane, (b) encapsulation of hydrophilic NPs into the liposomal aqueous core, and (c) surface adsorption or complexation mainly through electrostatic interaction or surface adsorption. Although several interesting examples of L−AuNP hybrids have been developed for either simple colloidal stabilization,[14,24] medical diagnosis,[25] or stimuli-responsive applications,[26−28] the efficient incorporation of metallic NPs into the liposomes remains the main challenge in the use and application of these systems.

Microfluidics (MFs) has emerged recently as a very promising technology for liposome fabrication. Compared to conventional liposome production methods, MFs offers precise control over liposome size and polydispersity,[29,30] and it is a very promising method for the preparation of lipid NPs encapsulating macromolecules such as siRNA and mRNA.[31−33] Furthermore, this control is achieved in a single step without the need for additional postproduction processing through extrusion or sonication. Very promising examples of liposomal systems with high payload capacity of hydrophilic and/or lipophilic drugs have been reported.[34−38] Moreover, advances in the design of integrated MF devices allow the combination of in-line liposome fabrication with other processes such as remote drug loading[39] and complexation with genetic materials such as pDNA and siRNA.[40] Signifi-Significantly, liposomes fabricated by MFs showed very similar or even improved physicochemical properties and biological functions such as increased transfection efficiency[40] and greater drug loading/retention[35,39] compared to liposomes prepared by traditional methods, while at the same time minimizing the steps required during processing saving several hours or days of work.[39,41] Here, we investigated the possibility of using MFs to encapsulate metallic NPs in the liposomes for imaging applications or modulation of drug release properties when combined with therapeutic molecules.

In this study, we aim to improve the incorporation of metallic NPs into liposomes using a MF-assisted self-assembly process. For this purpose, hydrophobic AuNPs of size 2−4 nm were selected as model NPs for incorporation into liposomes. The incorporation of increasing concentrations of AuNPs (0.025, 0.25, and 2.5 mg/mL) into liposomes (total lipid concentration is 4.5 mg/mL) was studied using MF and directly compared to L−AuNP hybrids prepared by the reverse-phase evaporation (REV) method. Physicochemical properties, encapsulation capacity, and morphology of L−AuNP hybrids prepared by the two methods were compared. In addition, the effect of AuNP incorporation on the lipid membrane rigidity and thickness was investigated.

■ EXPERIMENTAL SECTION

Materials. Hydrogenated soy phosphatidylcholine (HSPC) and 1,2-distearoyl-sn-glycero-3-phosphoethanolamine-N-[methoxy-(polyethylene glycol)-2000] (DSPE-PEG$_{2000}$) were kind gifts from Lipoid GmbH (Ludwigshafen, Germany). Chloroform and methanol were purchased from Fisher Scientific (Loughborough, UK). 1,6-Diphenyl-l,3,5-hexatriene (DPH) was supplied from Invitrogen (Paisley, UK). Phosphate-buffered saline (PBS), Sepharose CL-4B, 2 w/v % octanethiol-functionalized AuNPs in toluene, diethyl ether, 8-anilino-1-naphthalenesulfonic acid (ANS), aqua regia (HNO$_3$/HCl 1:3 v/v), and tetrahydrofuran were all obtained from Sigma-Aldrich (Dorset, UK). Milli-Q water (Millipore Milli-Q, Watford, UK) was used throughout the study. D$_2$O (>99.9% purity) was purchased from Aldrich (Dorset, UK).

Preparation of L−AuNP Hybrids by the MF Method. L−AuNP hybrids were self-assembled using the automated MF Asia 320 system (Syrris, Royston UK). First, a solution of AuNPs in CHCl$_3$ was prepared by evaporating (BÜCHI, Switzerland) toluene in which AuNPs were already dissolved and by resuspending the NPs in CHCl$_3$. Three different concentrations of AuNPs dispersed in CHCl$_3$ (1 mL) were then mixed with a 95:5 mol/mol solution of HSPC/DSPE-PEG$_{2000}$ (predissolved in 1 mL of MeOH) as shown in Table 1.

Table 1. Theoretical Concentration of AuNPs Used for the Preparation of L−AuNP Hybrids

formulation designation	total lipid concentration (mg/mL) HSPC/DSPE-PEG$_{2000}$ (95:5 mol/mol)	AuNPs (AuNPs) (mg/mL)
L−AuNP 0.025	4.5	0.025
L−AuNP 0.25	4.5	0.25
L−AuNP 2.5	4.5	2.5

Following the mixing of the AuNPs with the lipids, CHCl$_3$ was evaporated using a rotary evaporator at 460 mbar for 20 min at 40 °C. The resulting methanolic suspension of lipids and AuNPs was then further diluted with MeOH to a total lipid concentration of 1 mg/mL before introducing it into the Asia MF system. Note that preliminary studies had showed that higher lipid concentrations than 1 mg/mL resulted in the production of larger-sized liposomes. Once in the MF setup, the methanolic mixture containing both the lipids and AuNPs was mixed with an aqueous solution (PBS, pH 7.4) in an Asia 26 μL micromixer reaction chip (Syrris part number: 2101411—internal main channel cross section of 125 × 350 μm, internal mixing channel cross section of 50 × 125 μm). The optimum mixing conditions were determined by first exploring different flow rates such that an organic/aqueous flow rate ratio (FRR) of either 1:5 or 1:10 was used along with a total flow rate (TFR) of either 220, 330, 680, 1370, or 2750 μL/min (as described in Table 2). Optimization was initially explored using plain ("empty") liposomes and finalized with L−AuNP systems.

Once prepared, L−AuNP hybrids were then dialyzed for 24 h using a Spectra-Por Float-A-Lyzer (MWCO of 10 kDa) against PBS in order to remove any residual methanol. Following dialysis, a concentration step was performed using centrifugal Vivaspin column 20 to concentrate the final L−AuNP formulations to a total lipid concentration of 4.5 mg/mL as confirmed by the Stewart assay.[42]

Table 2. MF Parameters Used in the Study

| | organic/aqueous FRR | | | |
| | organic/aqueous = 1:10 | | organic/aqueous = 1:5 | |
TFR (μL/mL)	organic flow rate (μL/mL)	aqueous flow rate (μL/mL)	organic flow rate (μL/mL)	aqueous flow rate (μL/mL)
220	20	200	45	175
330	30	300	65	265
680	60	620	135	545
1370	120	1250	275	1095
2750	250	2500	550	2200

Preparation of L−AuNP Hybrids by the REV Method. L−AuNP hybrids were prepared using the REV methodology as previously described[43] using the same lipid composition and the same initial concentration of AuNPs (i.e., 0.025, 0.25, and 2.5 mg/mL), denoted as L−AuNP 0.025, L−AuNP 0.25, and L−AuNP 2.5, respectively. In brief, the required amount of hydrophobic AuNP dispersion was first added to a round-bottom flask. The organic solvent (toluene) in which the AuNPs were dispersed was then removed using rotary evaporation at 6 mbar and 40 °C for 30 min. The lipid mixture of 95:5 molar ratio of HSPC/DSPE-PEG$_{2000}$, dissolved in a 4:1 v/v mixture of chloroform/methanol, was then added, and the organic solvent was evaporated to form the lipid film containing the NPs. The AuNP-containing lipid film was then redissolved in 6 mL of 1:1 v/v chloroform/diethylether. Following this step, 1.5 mL of PBS was added, and the resultant mixture was bath-sonicated for 15 min at 40 °C, after which the organic solvents were removed using rotary evaporation at 460 mbar and 40 °C for 2 h. The large unilamellar liposomes formed by this process were then reduced in size by 30 min bath sonication at 60 °C.

Characterization of L−AuNP Hybrids. The apparent hydrodynamic radius and polydispersity index (PDI) of the liposomes were measured using Zetasizer Nano ZS (Malvern, Instruments, UK). Measurements were performed at 25 °C after dialysis against PBS of the L−AuNP hybrids prepared with the MF methodology.

Quantification of Lipid Concentration by Stewart's Assay. The concentration of lipid in the final products was assessed using the Stewart assay.[42] In brief, the liposome sample (20 μL) was mixed with Stewart's reagent (0.5 mL) and CHCl$_3$ (1 mL). The resultant mixture was shaken for 20 s and centrifuged at 13 793 RCF (Heraeus Biofuge 13), and the absorbance of the lipid-containing CHCl$_3$ layer was measured at 485 nm and compared to a standard curve prepared by plotting the absorbance at 485 nm versus lipid concentration in the range between 0.02 and 5 mg/mL.

Quantification of AuNP-Loading Efficiency by Ultraviolet Spectroscopy and Inductively Coupled Plasma Mass Spectrometry. The amount of Au and, by implication, the amount of AuNPs loaded into the liposomes were quantified using both ultraviolet (UV) spectroscopy and mass spectrometry. The UV absorbance of Au was recorded on Cary 50 UV−vis (Agilent Technologies, US) with the value of the maximum absorbance measured at 510 nm (after correction for any light scattering) being used to quantify the amount of Au present by comparison to a standard calibration curve. For inductively coupled plasma mass spectrometry (ICP−MS) measurements, samples were first dissolved in 1 mL of aqua regia, followed by a brief mixing for 30 s. The sample (100 μL) in aqua regia was then diluted with Milli-Q water up to 5 mL (thereby making an aqua regia concentration of 2% v/v) before performing ICP−MS (Agilent Technologies 7500 cx). The loading efficiencies of L−AuNP hybrids were then expressed as Au/lipid w/w %.

Separation and Characterization of L−AuNP Hybrid Fractions from Plain Liposomes. In order to separate and quantify the fraction of L−AuNP hybrids from the empty or plain liposomes contained in each sample, a centrifugation step was applied. Specifically, samples of L−AuNP hybrids loaded with different concentrations of AuNPs were centrifuged at room temperature for 2

h at 13 793 RCF (Biofuge 13). Characterization of L−AuNP hybrid fraction (assumed to be the sediment observed under the conditions of the test) and the unloaded empty liposomal fraction (assumed to remain suspended in the supernatant under the conditions of the test) was performed by measuring the ratio of AuNPs/lipids present in each fraction using a combination of UV spectroscopy and the Stewart assay. Any differences in size and PDI between the NPs present in the two fractions were also determined as described above.

Centrifugal Field Flow Fractionation Measurements. Centrifugal field flow fractionation (C-FFF) measurements were performed using a CF2000 C-FFF system (Postnova Analytics, Landsberg, Germany) which was coupled online to four detection instruments, namely, (1) a UV−vis spectrometer at 500 nm (S3210, Laserchrom, Rochester, UK), (2) a multiangle laser light scatterer (MALLS, Viscotek SEC-MALS20, Malvern Instruments, Worcestershire, UK) equipped with a laser operating at 532 nm, (3) a refractometer (Optilab T-rEX, Wyatt Technology, Dernbach, Germany) equipped with a laser operating at 633 nm, and (4) a dynamic light scatterer (DLS, Zetasizer Nano SZ, Malvern Instruments, Worcestershire, UK). The dimensions of the channel used were channel thickness, w = 237 μm, channel area = 100 cm^2, void volume (V_0) = 2.597 mL, radius of rotation (r) = 10.01 cm (according to the manufacturer's specification).

In a typical experiment, 20 μL of the sample was loaded in the injector loop, and the sample was injected over 114 s with a rotor speed equal to 4900 rpm. After 5 min relaxation time, the sample was then eluted in PBS at a rate of 0.5 mL/min. The method-wizard of the CF2000 control software (version 1.0.2.2, Postnova Analytics) was used for automatic decay field calculations. The rotor speed at each time point (RPM$_t$) is expressed in eq 1

$$RPM_t = RPM_0 \left[\frac{t_1 - t_\alpha}{t - t_\alpha} \right]^4 \tag{1}$$

where RPM$_0$ = starting rotor speed, t_1 = length of time for which RPM$_0$ is kept constant, t is the time expressed in minutes, t_α is an arbitrary constant expressed in minutes that can be tuned in order to modulate the decay rate, t_{tot} = decay time (the total duration of the elution being t_{tot} + t_1). All samples, except for the MF L−AuNP hybrid 2.5, were eluted using the following parameters: RPM$_0$ = 4900, t_1 = 10, t_α = −21, and t_{tot} = 49. In contrast, the MF L−AuNP hybrid 2.5 were eluted using parameters of RPM$_0$ = 4900, t_1 = 7, t_α = −35, and t_{tot} = 111.

The apparent hydrodynamic diameter (Z-average size) of the eluted particles was measured by DLS in flow mode, and the resulting chromatogram was analyzed using the DLS analysis tool of the Zetasizer Software (version 7.11, Malvern).

C-FFF allows the separation of particles based on mass and apparent hydrodynamic diameter (d_H).[39] According to the C-FFF theory, the force applied on a single particle (F) can be expressed as described in eq 2

$$F = \frac{\pi}{6} d_H^3 \Delta\rho G \tag{2}$$

where $\Delta\rho$ is the difference in apparent density between L−AuNPs and the solvent in which they are dispersed and G is the gravitational acceleration defined in eq 3

$$G = \left(\frac{2\pi \cdot RPM_t}{60} \right)^2 r \tag{3}$$

The retention time (t_r) is proportional to the force F according to eq 4

$$t_r = \frac{FwV_0}{6kT\dot{V}} \tag{4}$$

where w = channel thickness, V_0 = void volume, k = Boltzmann coefficient, T = absolute temperature, and $\dot{V}$ = channel flow rate. |$\Delta\rho$| for each time point can, therefore, be determined from a knowledge of the parameters r, V_0, and w, the method used for the elution (RPM$_t$

and $\dot{V}$), and the apparent hydrodynamic size of the particles determined during elution.

Transmission Electron Microscopy and Scanning Transmission Electron Microscopy Studies. Transmission electron microscopy (TEM) and scanning TEM (STEM) studies were performed by depositing 10 μL of L−AuNP hybrid dispersion onto a carbon-coated grid and staining with 1% w/v uranyl acetate solution. Excess liquid was removed by drying with a wick of filter paper and leaving the grids dry for 10 min. TEM images were acquired on a FEI (US) Tecnai 12 BioTWIN transmission electron microscope. Images were acquired with a Gatan Orius SC1000 CCD camera. STEM imaging was carried out using a FEI (US) Titan G2 80-200 transmission electron microscope fitted with a probe side aberration corrector and a high brightness X-FEG electron source operating at 200 kV.

X-ray energy-dispersive spectroscopic (XEDS) measurements were performed on the FEI Titan microscope using the FEI SuperX system ($\approx$0.7 sR collection angle) with a probe current of 360 pA. High-angle annular dark-field (HAADF) images were acquired using an inner collection angle of 62 mrad and a probe convergence angle of 21 mrad. Processing the XEDS dataset was performed with the HyperSpy software.[44] Principal component analysis was used to denoise the hyperspectral datasets with 3−4 components being used to reconstruct the data. The Au and uranium (U) elemental maps were obtained by integration of signal in the L lines at 9.71 and 13.61 keV, respectively.

Cryo-Transmission Electron Microscopy. Visualization of the samples with cryo-TEM was performed to study the morphology of L−AuNP hybrids and to confirm the incorporation of metallic NPs. Samples were vitrified by applying a 3 μL aliquot to a previously glow-discharged 200-mesh hole and Quantifoil carbon grids (Ted Pella, USA). Grids were blotted and then plunged into liquid ethane using a FEI Vitrobot Mark IV (FEI Company, the Netherlands). The samples were imaged by bright-field TEM using a Tecnai G2F20 microscope (FEI Company, the Netherlands) equipped with a Schottky Field Emission electron source and a US1000 2k × 2k Gatan CCD camera operating at an acceleration voltage of 200 kV. The cryo-tomographic (CET) tilt series were collected on the vitrified sample by tilting over ±60° in 2° steps. Computation of tomograms and postprocessing were performed using the IMOD 4.9.2 software package.[45] Segmentation by isosurface and 3D visualization were undertaken using the Amira package (FEI Visualization Science Group, Bordeaux). Cryo-TEM and CET imaging were both performed under low dose conditions, with a total dose of 60−80 electrons/Å^2 being used for the whole tilt series.

Fluorescence Anisotropy Measurements. Fluorescence anisotropy experiments were performed to study the effect of metallic NP incorporation on the liposome's membrane fluidity. The hydrophobic probe, DPH, and the hydrophilic probe, ANS, were used to monitor the changes in the fluidity of the hydrophobic region of the lipid membrane and near the liposome's surface, respectively. Experiments were performed as previously described.[46] Briefly, L−AuNP hybrids were further diluted to a total lipid of 0.025 mM total and divided into two 4 mL aliquots. Either a DPH in tetrahydrofuran solution (0.8 mM, 2.5 μL) or an aqueous ANS solution (10 mM, 4 μL) was mixed with the liposomes at 500:1 total lipid/DPH or 25:1 total lipid/ANS. To allow the probes to be incorporated, the samples were shaken at room temperature for 2 h and then left overnight before starting the measurements. Fluorescence polarization was then measured by a Carry Eclipse, Agilent technology equipped with an automated polarizer and a thermostatic cell holder connected to a water bath to control the sample temperature. For the experiments utilizing DPH, the anisotropy measurements were performed using an excitation wavelength of 395 nm (slit of 10 nm) and an emission wavelength of 476 nm (slit of 5 nm). Measurements were started at 25 °C, and then the temperature was increased gradually up to 65 °C at a step change of 3 °C. The samples were equilibrated for at least 2 min after each temperature change. Fluorescence anisotropy was then measured automatically by the spectrofluorometer using eq 5

$$r = \frac{\text{Iv}_\text{v} - \text{GIv}_\text{H}}{\text{Iv}_\text{v} + 2\text{GIv}_\text{H}} \tag{5}$$

where r = fluorescence anisotropy and Iv_V and Iv_H = the emission intensity excited with vertically polarized light and measured with an emission polarizer oriented in a parallel or perpendicular direction to the plane of excitation, respectively. G = an instrument specific factor calculated to correct the instrument polarization, which is equal to $I_{\text{HV}}/I_{\text{HH}}$, and obtained by measuring the vertically and horizontally polarized emission intensities after excitation with horizontally polarized light. A sigmoidal Boltzmann curve was fitted to the experimental values were performed using Origin 8.5 software.

Small-Angle Neutron Scattering Measurements. Small-angle neutron scattering (SANS) measurements on vesicles (prepared using the REV methodology) without a NP payload and L−AuNP hybrids prepared by both MF and REV methodologies were performed using the beam line, SANS2D, at the ISIS pulsed neutron source (STFC Rutherford-Appleton Laboratory, Didcot, UK). All samples were prepared in PBS and diluted before measurement with an equal volume of PBS in deuterium oxide (D$_2$O) in order to provide the contrast (or scattering length density difference) necessary for the SANS measurements. The empty lipid vesicles and the L−AuNP hybrids were measured at a total lipid concentration of 0.5 mg/mL in 1 mL bango cells using a solvent of composition of 1:1 v/v PBS$_{\text{H}_2\text{O}}$/ PBS$_{\text{D}_2\text{O}}$ and at 25 °C. Note that, with the exception of D$_2$O, all the components used to make PBS$_{\text{D2O}}$ were protiated.

The SANS intensity, $I(Q)$, of the samples was measured as a function of the scattering vector as described in eq 6

$$Q = (4\pi/\lambda)\sin(\theta/2) \tag{6}$$

where $\theta/2$ = the scattering angle. The data were normalized to the appropriate sample transmission after subtraction of the scattering of the relevant solvent which was normalized to its corresponding transmission. The fitting of the SANS data always included a flat background correction to allow for any mismatch in the incoherent and inelastic scattering between the sample and the solvent, with the levels of the fitted background being checked to ensure that they were physically reasonable. The SANS data obtained in the present study were well modeled assuming a mixture of (isolated/single) infinite planar (lamellar) sheets with the addition of one-dimensional paracrystals (stacks) to account for the presence in the sample of any multilamellar vesicles. The fits to the SANS data were obtained by the least-squares refinement of seven parameters, namely, the mean bilayer thickness (L), the Lorentz factor (R_σ), the number of bilayers in the stack (M), their mean separation or d-spacing (D), the width of the Gaussian distribution in the plane ($\sigma(D)/D$), and the absolute scale factors for the unilamellar and multilamellar vesicles. During the analysis of the SANS data in the present study, the following factors, namely, $\sigma(L)/L$, $\sigma(D)/D$, and R_σ were fixed at 0.1, 0.05, and 200, respectively. The only exception was the L−AuNP prepared using the MF methodology where the value of R_σ had to be increased to 560 to satisfactorily fit the data; a lower value R_σ would not produce a reasonable fit of the data. In addition, when modeling the SANS data using a mixed population of sheets and stacks, L, $\sigma(L)/L$, and R_σ were constrained to be the same for the isolated/single and stacked lamellae, a not unreasonable assumption. All the SANS data were fitted using a multilayer stack comprising 3−4 bilayers. For all models, the least-squares refinements were performed using the model-fitting routines provided in the FISH software.[47]

Atomic Force Microscopy. Atomic force microscopy (AFM) analysis was performed to study the effect of NP incorporation on the bilayer thickness. L−AuNP hybrid dispersion (20 μL) loaded with 2.5 mg/mL of AuNPs and formulated via REV or MF methods were deposited on the surface of a sheet of freshly cleaved mica and were allowed to adsorb for 1 min. Nonadsorbed liposomes were washed off by filtered distilled water. Samples were then dried with dust-free argon gas. A Molecular Force Probe 3D AFM (MFP-3D, Asylum Research, Oxford Instruments, Abingdon, UK) equipped with a ScanAsyst-Fluid cantilever (Bruker, Camarillo, CA, USA) was used to
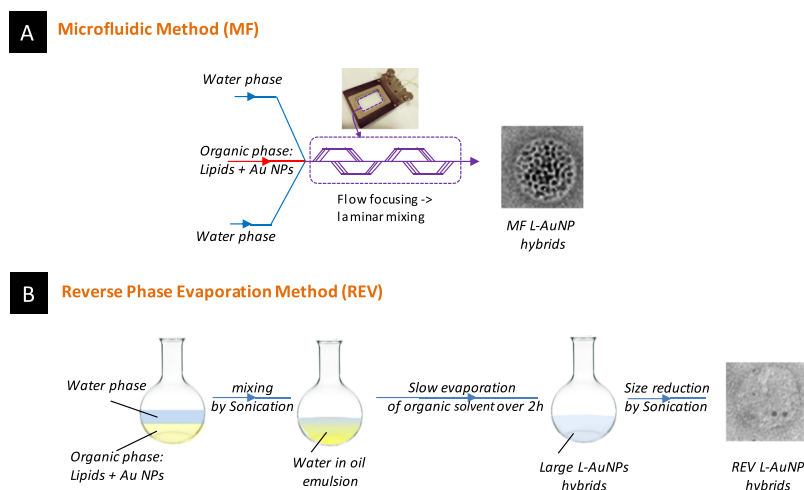
Figure 1. Schematic representation of L−AuNP hybrid production by the (A) MF methodology and (B) REV methodology showing the different steps involved in each method. No size reduction step is needed for L−AuNP hybrid production via the MF method, while liposome size is reduced by sonication for production with the REV method.

acquire the AFM images in air at room temperature in tapping mode. The silicon nitride cantilever had a nominal spring constant of 0.7 N/m and a typical resonance frequency of 150 kHz. Different areas of the samples (<10 μm^2) were imaged at a scan rate and a resolution of 1 Hz and 512 × 512 pixels, respectively. Images were analyzed with MFP-3D software (Oxford Instrument), and profiles were plotted with Origin 8.5 software.

■ RESULTS AND DISCUSSION

Fabrication and Physicochemical Characterization of L−AuNP Hybrids. MFs represent a promising technology for the scalable production of both NPs and liposomes offering the possibility of a precise control over their size and polydispersity as well as the potential to increase the drug-loading capacity.[29,36,48,49] When the organic and buffered aqueous phases are mixed in a MF system, the polarity of the solvent increases gradually when compared to the polarity of the organic solvent in which the phospholipids were dissolved. As a consequence, the solubility of the phospholipids progressively reduces promoting their self-assembly into planar bilayer disk-like structures. These planar structures eventually close up into spherical vesicles or liposomes.[36,50] In the present study, L−AuNP hybrids were fabricated through self-assembly using either MF (Figure 1A) or REV methodology (Figure 1B). Specifically, the incorporation of three different concentrations of AuNPs, namely, 2.5, 0.25, and 0.025 mg/mL, into self-assembled liposomes comprising HSPC/DSPE-PEG$_{2000}$ (95:5) mol/mol has been investigated. To obtain the best level of incorporation of AuNP into the lipid bilayer, hydrophobically derivatized AuNPs of 2−4 nm size were used.[13,22] The conditions for the MF preparation of the L-AuNP were optimized using an automated Asia 320 MF system (Syrris, Royston UK) equipped with an Asia 26 μmixer reaction chip. PBS was selected as the solvent for the aqueous phase because previous work had found that liposomes composed of 1,2-distearoyl-sn-glycero-3-phosphocholine lipids have smaller size when prepared in PBS buffer compared to that in other buffers such as tris buffer.[36] The choice of the organic solvent plays a crucial role in the defining properties of the resultant liposomes including their size and stability. For example, the use of methanol, as is the case here, and isopropyl alcohol as solvents produces superior liposomes compared to the use of methanol

as a solvent. This is the result of the tendency of ethanol to promote vesicle fusion and consequently liposome aggregation if it is not completely removed.[51] Methanol was selected as an organic solvent for two reasons, namely, it dissolves both HSPC and DSPE-PEG$_{2000}$ and because it is miscible with the PBS buffer. However, because the hydrophobic AuNPs, supplied suspended in toluene, have a tendency to aggregate in methanol, extra steps had to be incorporated into the MF preparation process in order to ensure that NPs were fully suspended. Consequently, after the evaporation of the toluene-dispersing solvent, the AuNPs were resuspended in CHCl$_3$ and mixed with the methanolic lipid solution and sonicated for 20 s in order to obtain a homogenous NP dispersion. CHCl$_3$ was then removed from the sonicated mixture by 15−20 min evaporation at 460 mbar and at 40 °C before the final AuNP lipid mixture was introduced into the MF system. TEM images of the AuNP before and after evaporation of toluene and after resuspension in CHCl$_3$ confirmed the absence of AuNP aggregates (Figure S1A,B). HSPC was specifically selected as the major lipidic component of the liposomes because earlier studies had demonstrated that lipids with long hydrophobic chains exhibited a higher capacity for the incorporation of hydrophobic molecules.[52,53] In the same vein, cholesterol was not added to the formulation as it had been shown to reduce metallic NP incorporation into lipid bilayers.[54,55] However, cholesterol is well known to have a significant effect on the structural stability and drug retention inside the liposomes under physiological condition. Thus, the effect of cholesterol on metallic NP loading into the liposomes should be considered.

In agreement with earlier studies, we observed that the FRR, which represents the organic/water ratio at the mixing point, affects the size of the liposomes produced. In the present study, two FRRs, namely, 1:5 and 1:10, were investigated. When the FRR is increased from 1:5 to 1:10, the increased volume of the aqueous solvent imposes a dilution on the organic solvent facilitating a rapid mixing[56] and thereby favoring the formation of small liposomes.[37,49,54] On the other hand, when a FRR of 1:5 was used, irrespective of the TFR and the running temperature, the resultant particles exhibited a bimodal distribution with a Z-average size of greater than 800 nm (data not shown). In contrast, when an FRR equal to 1:10 was
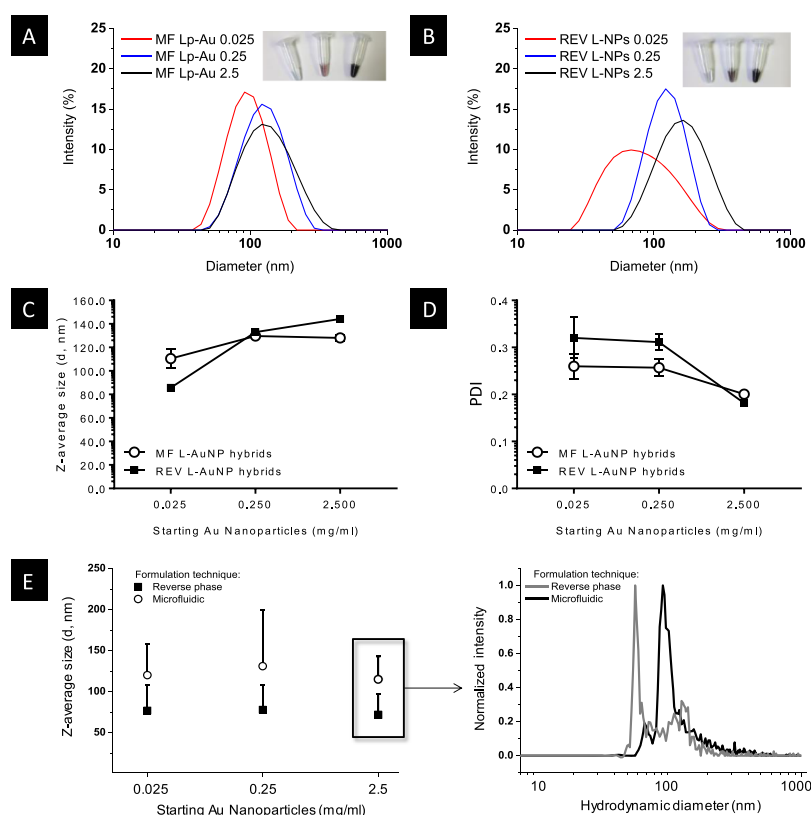
Figure 2. L−AuNP hybrid characterization via photographic images and intensity distribution measurements as determined by DLS prepared by the (A) MF and (B) REV methods using different initial amounts of AuNP, namely, 0.025, 0.25, and 2.5 mg/mL; (C) mean Z average apparent hydrodynamic diameter and (D) PDI of the corresponding L−AuNP, respectively; (E) mean Z average apparent hydrodynamic diameter of L−AuNP hybrids after separation by C-FFF and the corresponding intensity distribution of the L−AuNP prepared using the highest initial concentration of AuNPs. Error bars refer to the width of the distribution. Samples are measured at 25 °C, n = 3.

used, liposomes characterized by small sizes and low PDI values were observed when a TFR of less than 680 μL/min and a running temperature of equal to or greater than 60 °C were used (Figure S1C). This result was in contrast to that of other researchers[56,57] who have reported that the TFR used has little effect on the final size of the liposomes produced.

Additionally, the size of the liposomes was decreased by an increase in the experimental temperature up to 65 °C (i.e., the temperature at which the micromixer chip was maintained during the mixing of the two phases) to above the T_m of the lipids (∼50 °C) as determined by our anisotropy measurements and from the previous literature.[58,59] This effect of temperature is a consequence of the higher mobility of the phospholipid tails, which results in the efficient, rapid mixing of the solvents in the chip, especially at the lower FRR. In this context, it is worth mentioning that for a TFR ≥ 1370 μL/min, the residence time of the solvents in the micromixer channels prior to mixing is insufficient to ensure temperature equilibration. Therefore, at TFR values above 1370 μL/min (values between 680 and 1370 μL/min were not tested) mixing was not favored mainly because the actual experimental temperature was less than T_m. This observation could explain why increasing the TFR above 680 μL/min resulted in the production of liposomes of an increased size. A better control of the size at higher TFR could be possible by simply changing the geometry of the mixing chip.

On the basis of the observations made in the present study, the L−AuNP hybrids were routinely prepared using a FRR of 1:10, a TFR of 220 μL/min, and a running temperature of 65 °C.

In order to evaluate the benefits and drawbacks of using the MF technology for the production of L−AuNP hybrids, L−AuNP hybrids of comparable composition to those prepared using MF were prepared using the REV methodology (Figure 1B),[43,60] a method widely used for the preparation of L−AuNP hybrids. Significantly, no (liposomal) size reduction step was required when using the MF methodology, which is an advantage over the REV method which requires a reduction in liposomal size, here performed by 30 min of bath sonication at 60 °C. Characterization of the L−AuNP hybrids using DLS (Figure 2A−C) showed that the MF methodology produced L−AuNP hybrids with a more homogeneous size distribution (i.e., a narrower PDI) compared to those prepared using the REV method (Figure 2D). These size data were confirmed by C-FFF, which showed that the REV method resulted in the production of a larger proportion of smaller-size liposomes when compared to the single homogenous peak of approximately 100 nm recorded for the liposomes prepared using the MF method (Figure 2E).

The ability to finely tune all these parameters in the MF setup enables controlled mixing of the liquid interfaces to achieve the desired properties (e.g., size and PDI) of the final liposome product. This can be achieved in a single process without the need for postprocessing or changing the lipid composition of the liposomes.[30,35] Cancer therapy is one example where size reduction of liposomes is desirable.[34] A recent study by Dong et al. demonstrated that by using the MF
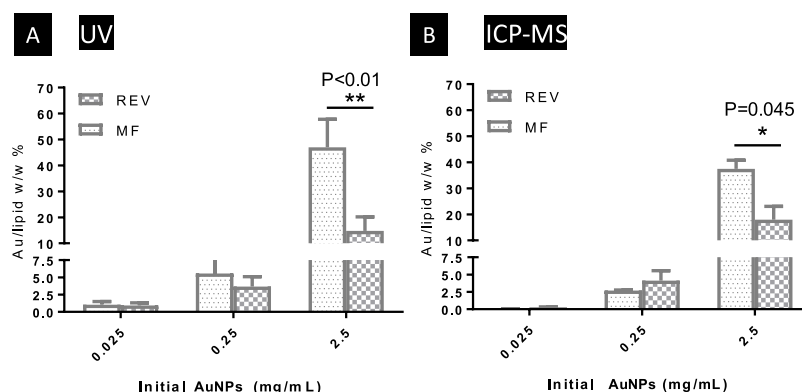
Figure 3. Quantification of the loading capacity of L−AuNP hybrids by the MF and the REV methods with different initial amounts of AuNP, namely, 0.025, 0.25, and 2.5 mg/mL as determined by (A) UV−vis spectrophotometry and (B) ICP−MS. Data are expressed as a wt % gold (Au) per wt lipid. Quantification of lipid concentration in each sample was performed by Stewart's assay. Samples measured at room temperature, $n = 3$ for UV measurements and $n = 2$ for ICP−MS measurements.

methodology, it was possible to reduce the size of doxorubicin-loaded liposomes to 50 nm. As a result of that, improvement in tumor extravasation and intratumoral distribution was observed.[34]

Quantification of L−AuNP Hybrid Loading by UV−Vis and ICP−MS. Another advantage of the MF production of liposomes is the enhanced capacity for their payload of therapeutic molecules. Interestingly, the payload capacity of hydrophilic drugs is almost doubled with the MF technology compared to less than 10% obtained by traditional liposome preparation methods.[1] Moreover, the MF technology is highly efficient for incorporation of poorly water-soluble drugs into the liposomes and has demonstrated the potential for entrapping both hydrophilic and lipophilic drugs simultaneously. Efficient loading of a wide range of therapeutics has been reported. These include hydrophilic molecules (e.g., metformin, sulforhodamine)[36,61] and hydrophobic molecules (e.g., glipizide and propofol)[36,58] either individually or in combination.[36] The aim of the present study was to explore the use of MFs for the fabrication of L−AuNP hybrids because of the poor payload capacity reported with other traditional methods.[62] The quantification of AuNPs embedded in the liposomes was performed using UV−vis spectrometry (Figures 3A and S2) and ICP−MS (Figure 3B). Regardless of which of the assay methods was used, an increase in AuNP loading into the liposomes with increasing initial AuNP concentration was observed. Significantly, a 3-fold increase in loading efficiency was observed in the hybrid systems prepared by the MF methodology when compared to the REV method at the highest initial concentration of AuNP examined, that is, 2.5 mg of AuNPs. In comparison, no difference in the AuNP-loading capacity between the two methods was observed at the lower initial AuNP concentrations of 0.025 and 0.25 mg, although qualitative differences (discussed in the next paragraph) were observed in TEM images (Figure 4A,B).

Size exclusion chromatography (SEC) was used to separate AuNPs that were not incorporated into liposomes. Quantification of the amount of phospholipid and Au and therefore, by implication, the amount of AuNPs in each fraction eluted indicated that the AuNP elution mirrors that of the liposomes (as assessed by phospholipid concentration) with very small amounts of AuNPs being detected in the other fractions, suggesting that the majority of AuNPs were incorporated into the liposomes, that is, there were very minimum free AuNPs

(Figures S3 and S4). This was also confirmed with TEM imaging of L−AuNP before and after elution through the sepharose CL-4B column, which confirmed that no free AuNP aggregates exist before purification and suggested that most of the AuNPs already incorporated into the liposomes (Figure S4C,D). This was consistent for all the L−AuNP samples prepared by the MF and REV methodologies. Correction of any loss of lipid vesicles on the SEC was performed by measuring the lipid concentration with Stewart's assay. In addition, the separation of empty (i.e., AuNP-"free") liposomes from L−AuNP hybrids was explored by centrifugation during which the L−AuNP hybrids were sedimented because of the dense AuNPs they contained, while the empty liposomes remained suspended in the supernatant. Qualitative validation of these data was obtained using TEM imaging (Figure S5), which showed clearly the separation of the L−AuNP-containing liposomes from the empty liposomes. DLS measurements of the two fractions indicated, irrespective of the method of preparation, an increase in the apparent hydrodynamic size of the liposomes in the presence of AuNP with sizes in the range 130−260 nm being recorded for the L−AuNP hybrids compared to sizes of less than 100 nm for the empty liposomes (Table S1).

The hybrids were also analyzed by C-FFF, a technique which exploited both DLS and UV as detection methods which allowed the measurement of the apparent hydrodynamic size of particles and monitoring of the presence of any Au, respectively (Figure S5C). When comparing the total particle population, the measured UV signal of the various liposomal preparations was found to be almost 1 order of magnitude higher for L−AuNP hybrids using the MF methodology, indicating higher AuNP loading. Furthermore, the apparent difference in density ($\Delta\rho$) between the sample and solvent determined for the various liposomal preparations studied was particularly pronounced for the L−AuNP hybrids prepared using the highest initial concentration of Au of 2.5 mg/mL, with those prepared using MF exhibiting the highest density difference and therefore by implicating the highest concentration of AuNPs. The fraction of loaded and unloaded liposomes expressed as wt % of the total liposomes prepared by MF and REV was also calculated (Figure S5D). Data indicated that the fraction of loaded liposomes is higher for MF compared to that for REV for all AuNP concentrations tested.
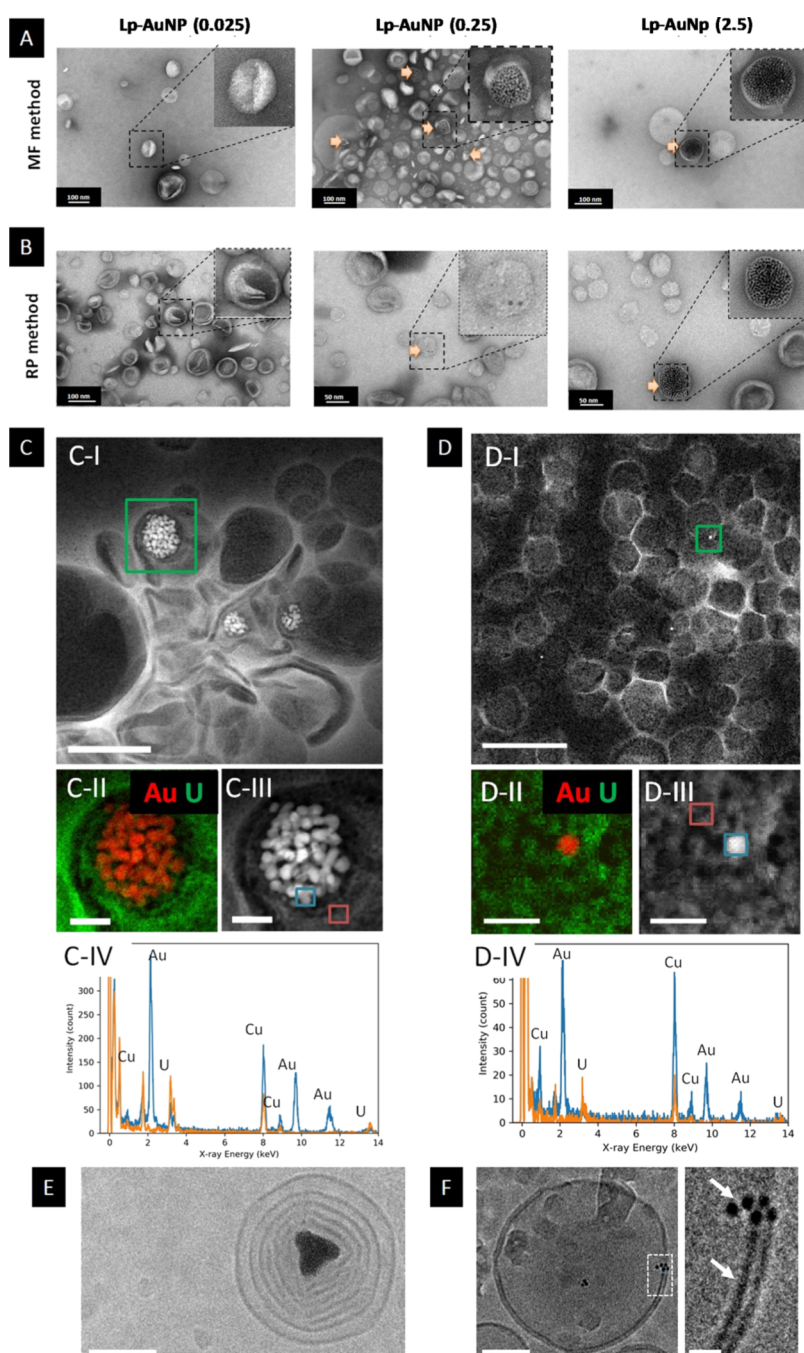
Figure 4. Characterization of L−AuNP hybrids by EM. TEM images of L−AuNP hybrids prepared by the (A) MF method and (B) REV method with different initial amounts of AuNP, namely, 0.025, 0.25, and 2.5 mg/mL. It was not possible using TEM to detect AuNPs in the liposomes with the lowest amount of AuNPs. HAADF image of L−AuNP hybrids 0.25 prepared by (C-I) MF and (D-I) REV methods highlighting inside the green box representative regions of with liposomes containing aggregates of AuNPs (MF method) and a small number of individual nanoparticles (REV method). Au−L and U−L composite elemental (Au and U) maps obtained by XEDS and simultaneously acquired HAADF images of the highlighted area of L−AuNP hybrids prepared by the MF method (C-II,C-III) and the REV method (D-II,D-III). XEDS spectra show Au from the AuNPs in blue and the area surrounding the AuNPs in orange. Cryo-EM images of L−AuNP hybrids prepared by the (E) MF method and (F) REV method with an initial amount of AuNP, namely, 2.5 mg/mL. The scale bar for (C-I,D-I) is 200 nm; for (C-II,C-III), it is 20 nm; for (D-II,D-III), it is 10 nm; for (E), it is 100 nm; and for (F), it is 50 nm (left) and 10 nm (right).

Qualitative Evaluation of L−AuNP Hybrids with Electron Microscopy. The morphological characterization of the L−AuNP hybrids was determined using TEM (Figure 4A,B). The resultant TEM images confirmed the incorporation of AuNPs into the liposomes. Furthermore, in agreement with UV−vis and ICP−MS measurements, the TEM images revealed a higher AuNP-loading capacity for the systems prepared by the MF method. Unfortunately, detection of AuNPs in the liposomes at the lowest initial concentration of Au was not possible. TEM images also revealed the presence of mixed population of both loaded and unloaded liposomes. The association of AuNPs with the liposomes was confirmed with STEM EDS microscopy (Figure 4C,D), which verified the association of Au with the liposomes by elemental analysis. A

tendency toward the formation of NP-rich domains was noticed in the MF L−AuNP hybrid samples compared to mainly individualized NPs present in the lipid bilayer of the REV L−AuNP hybrids.

To further probe the association of AuNPs with the liposomes, the L−AuNP hybrids were studied using cryo-TEM. Cryo-EM illustrates qualitative distinctions between the hybrid systems produced by the two methods when incorporating the highest initial amount of AuNPs. Specifically, the MF methodology provided hybrids that contained a core of AuNP aggregates (Figure 4E). In these systems, the core looks to be "wrapped" by a number of lipid bilayers which create a multilamellar structure around it. The cryo-TEM images of the MF-prepared L−AuNP hybrids indicated the coexistence of membrane-embedded and interdigitated (i.e., encapsulated NPs with some association of the internal lipid membrane) AuNP-rich domains, suggesting the structural stabilization of the AuNP hydrophobic interactions. These findings are in agreement with a recent work from the Cullis group that reported the use of MFs to encapsulate negatively charged AuNP inside positively charged L−NP. However, in their case, structural stabilization of the final system is through electrostatic interactions.[31] In contrast, the REV method was seen to result in the production of hybrids that predominately consist of two lipid bilayers and contain individual AuNPs or small aggregates of AuNPs (Figure 4F). Both unilamellar and multilamellar liposomes were seen in the hybrids regardless of their preparation methods. Further CET studies performed on the L−AuNP hybrids prepared by MF confirmed the incorporation of AuNPs in the liposomes (Figure 5 and
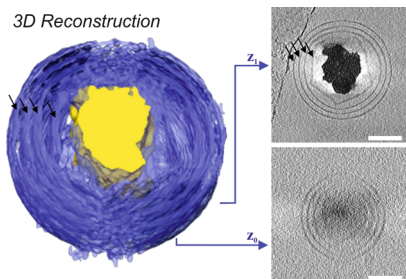
Figure 5. 3D model obtained from the cryo-tomography performed on a multilamellar liposome produced by the MF method. On the right, two z-stack images are provided. It was possible to observe the multilamellar structure (black arrows point the different phospholipid layers) and to demonstrate that the AuNP agglomerate is incorporated into the liposome. Scale bar = 100 nm. Note that the 3D model has been segmented in order to remove unwanted artifact (see Video S1).

Video S1). The ability to form a multilamellar shell is very interesting and could have other possible applications such as increasing the loading efficiency of hydrophobic drugs. However, the factors responsible for controlling the number of layers in those multilamellar systems and the effects of that on the physical properties of the final system need to be investigated. Nevertheless, because the % of NP incorporation into the lipid bilayer using the REV method is lower than MF, the overall effect of this incorporation on the lipid membrane fluidity is relatively minor.

Effects of AuNP Incorporation on Bilayer Thickness and Rigidity. The effect of the presence of the AuNPs on the properties of the hybrid systems was established using a combination of advanced biophysical tools, namely, fluorescence anisotropy, SANS, and AFM. Anisotropy is widely used to study the effect of NP incorporation on lipid membrane packing and fluidity because of its high sensitivity to size, position, concentration of NPs incorporated, and sensitivity to experimental temperature conditions.[63−65] As a reflection of this enhancement in AuNP incorporation, an increase in ANS fluorescence anisotropy values was observed, indicating a reduction in the membrane fluidity or a rigidifying effect close to the head group region of the lipid membrane (Figure 6A,C). This effect was observed throughout the temperatures tested (i.e., below and above the T_m of the lipid membrane), particularly in the case of the hybrids prepared using the MF methodology where there was a noticeable increase in anisotropy with initial AuNP concentration, suggesting that the bilayer rigidity close to the head group region was increased by increasing the concentration of AuNP. In the hybrid systems prepared using the REV method, the anisotropy values were reduced, and only in the case of the highest initial AuNP concentration, an increase was observed. Previous studies have demonstrated the ability of ANS molecules to penetrate the lipid bilayer and interact with the head group region on the inner and outer surfaces of the lipid bilayer.[66,67] Therefore, we expect the ANS anisotropy data to reflect the effect observed from both unilamellar and multilamellar vesicles in both methods. The effect of L−AuNP hybrids size on membrane curvature and lipid packing might also affect ANS anisotropy data and should be taken into consideration when interpreting the results.

On the contrary, minute changes were detected from DPH anisotropy, demonstrating minimum NP association with the core of the lipid membrane (Figure 6B,D). No significant effect of changing the initial AuNP concentration was detected on the T_m of the liposomes when prepared using either methodology ($T_m \approx 50$ °C for MF hybrids vs ∼46 °C for REV hybrids). The lower T_m recorded from REV hybrids could be due to the presence of residual solvents that interdigitate in the lipid bilayer and results in distortion of lipid packing and hence reduced T_m compared to MF hybrids. The findings in the current study agree with previous studies reporting that the incorporation of small hydrophobic NPs (<5 nm) increases membrane rigidity. On the contrary, NPs larger than 5 nm result in the distortion of the membrane effect, causing an increase in lipid membrane fluidity.[23,68]

In agreement with the anisotropy findings, SANS data (Figures 6E,F and S6, Table 3) indicated that the incorporation of AuNPs into the liposomes resulted in a slightly thicker ($L = 49.1 \pm 0.2$ vs 45.6 ± 0.1), more rigid bilayer ($R_\sigma = 560$ vs 200) in the hybrid systems fabricated by the MF method and containing the highest initial load of AuNPs when compared to the corresponding hybrids prepared by the REV method and the "empty" liposomes. This observation may be a consequence of the differences in the loading efficiency between the two methods. SANS also indicated the coexistence of both unilamellar and multilamellar vesicles for both methods with the amount of multilamellar vesicles present being lower in the vesicles prepared using the MF methodology (Table 3)—a result that correlates well with the cryo-TEM findings.

Surface topography of L−AuNP hybrids was examined by AFM. Profile analysis performed using the AFM images (Figure 7) indicated that AuNP incorporation increased the height (i.e., thickness) of the lipid bilayer from 4 to 5 nm
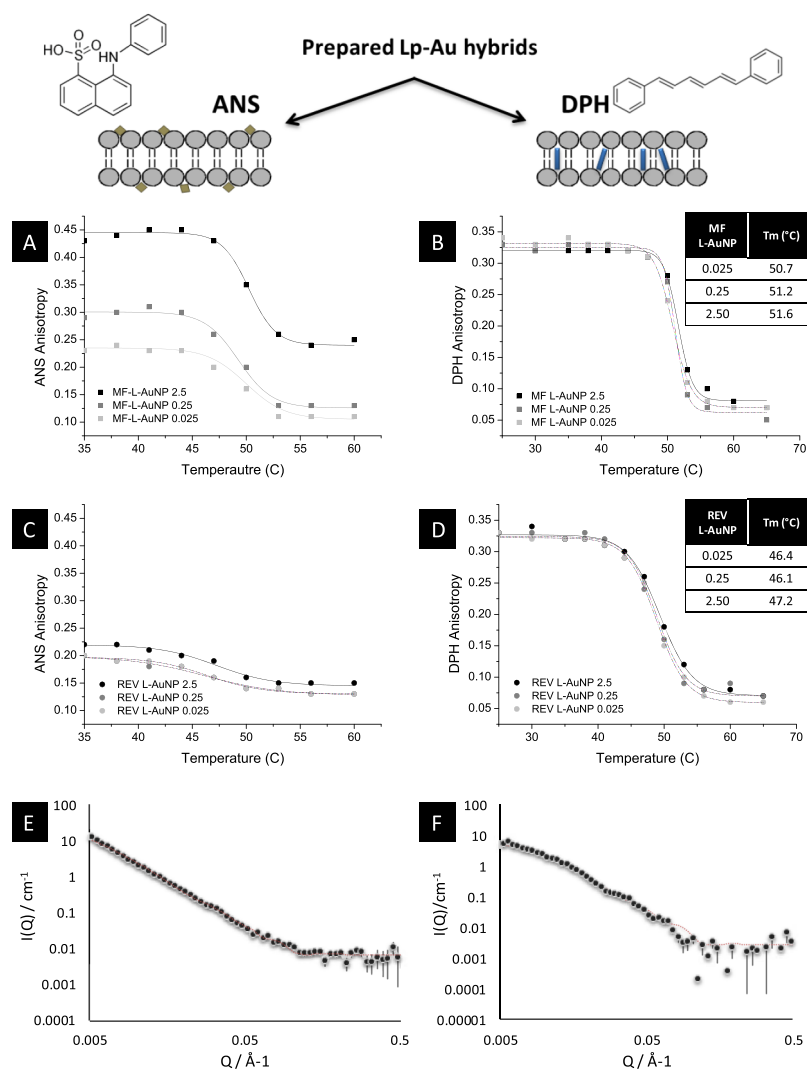
Figure 6. Variation of fluorescence anisotropy of ANS (A,C) and DPH (B,D) in L−AuNP hybrids prepared by the (A,B) MF and (C,D) REV methods using different initial AuNP concentrations, namely, 0.025, 0.25, and 2.5 mg/mL over the temperature range 25 °C until 65 °C. Fluorescent data of DPH anisotropy were fitted to obtain the phase transition temperature (T_m) as indicated by the inset tables in (B,D). SANS data (dots) and the best fit to the data (solid line) obtained using the mixed sheet and stack model for L−AuNP hybrids prepared by the (E) MF and (F) REV methodology measured at 25 °C.

Table 3. Structural Parameters Obtained through Fits to the SANS Data Obtained for Vesicle Dispersions Prepared from the Various Liposomal Preparations at 25 ± 0.1° C[a,b]

liposomal preparations	mean bilayer thickness (L) (Å)	the Lorentz factor ($R\sigma$) (Å)	mean separation or d-spacing (D) (Å)	number of bilayers in the stack (M)	ratio of unilamellar: multilamellar surface area
empty liposomes	45.6(0.1)	200	64.9 ± 0.2	3	1.5
MF L−AuNP 2.5	49.1(0.2)	560	72.5 ± 0.3	4	2.7
REV L−AuNP 2.5	45.6(0.1)	200	64.9 ± 0.2	3	1.4

[a]Symbols used are as described in the text. [b]For L, the figures in parentheses show standard errors; for D, the uncertainties reported represent the convolution of the statistical error on D and the value of the fitted polydispersity.

("empty" liposomes) to almost 8−10 nm (L−AuNP hybrids) for both preparation methods tested at the highest initial AuNP concentration. This result was in agreement with studies previously published by ourselves and others who reported an increase in the bilayer thickness after NP incorporation.[43,69]

Overall, our structural characterization corroborated the two proposed models of AuNP association with the liposomes, namely, the membrane embedded and the encapsulated

models. In agreement with TEM images, a mixed population of AuNP-loaded and -unloaded liposomes was detected. In the case of the MF L−AuNP hybrids, the coexistence of the lipid bilayer-embedded AuNPs (i.e., the membrane-embedded model) and AuNPs inside the liposomes (i.e., the encapsulated model) with some interaction with an internal lipid membrane was observed. In contrast, membrane-embedded AuNPs were found to exist in the majority of REV L−AuNP hybrids with a
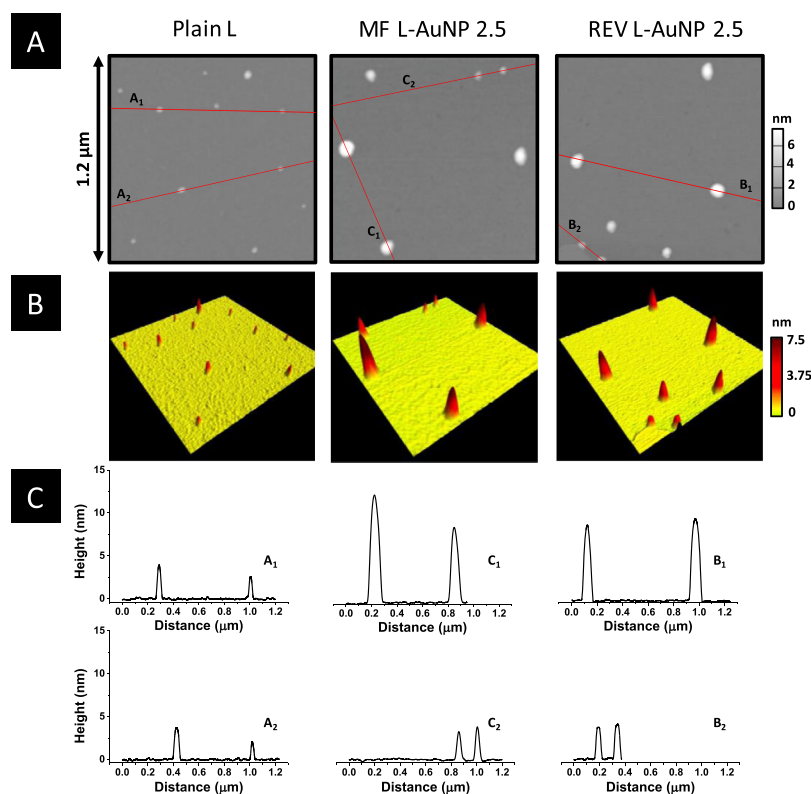
Figure 7. Characterization of empty liposomes (plain L) and L−AuNP hybrids (MF L−AuNP 2.5 and REV L−AuNP 2.5) by AFM showing (A) amplitude, (B) 3D images, and (C) cross-sectional analysis. Measurements performed at 25 °C.

minority of encapsulated AuNPs being observed. SANS and AFM observations reinforced anisotropy measurements that confirm the increase in the bilayer thickness for MF L−AuNP hybrid systems.

Optimization processes reported here are all based on one specific instrument (Asia 320 MF system). Whether the process can translate and expand to other types of MF systems requires further investigation.

Collectively, our results demonstrate that by using a MF method of preparation, we were able to improve the loading of hydrophobic metallic NPs into liposomes when compared to the traditional REV method. The results obtained in this study using a commercial MF system enable the reproducible, automated manufacture of L−AuNP hybrids. Other critical factors that may be worth exploring in the future are the effect this enhanced loading could have on the encapsulation efficiency of imaging and/or theranostic systems. More work needs to be undertaken to prove that the enhanced payload of AuNP observed in the L−AuNP hybrids can be translated into a higher efficiency for such systems. Moreover, the concentration of AuNP loaded inside the liposomes should be carefully selected to ensure that theranostic properties of AuNP are not lost because of possible aggregation if very high concentration is loaded.

CONCLUSIONS

We have demonstrated for the first time the fabrication of L−AuNP hybrids using automated MF technology. The L−AuNP hybrids prepared in the present study showed a more homogeneous size distribution and correspondingly smaller PDI compared to those made using the traditional REV methodology. Most significantly, the capacity of the NPs

prepared using the MF technology for its AuNPs payload was three times that of the REVs prepared using the traditional methodology. Detailed structural characterization of the L−AuNP hybrids using a range of advance biophysical methods confirmed the superiority of the MFs for the preparation of NP-containing liposomes. The data also revealed the coexistence of membrane-embedded and interdigitated NP-rich domains which are understood to be a consequence of both the size of the AuNPs studied and their hydrophobic nature. The present findings demonstrate the benefit that the MF technology offers in the preparation of hybrid NPs with improved fabrication and functionality and to expedite their translation for imaging and/or therapeutic purposes.

ASSOCIATED CONTENT

ⓈSupporting Information
The Supporting Information is available free of charge on the ACS Publications website at DOI: 10.1021/acs.langmuir.9b00579.

> TEM images of AuNPs under different conditions, standard curves for lipids and AuNP measurements, UV−vis spectra for AuNPs, purification process of L−AuNP hybrids using a sepharose CL-4B column, separation of L−AuNP hybrids from unloaded liposomes by centrifugation, SANS data (dots) for plain "empty" liposomes, and colloidal properties of L−AuNP hybrids (PDF)

AUTHOR INFORMATION

Corresponding Authors
*E-mail: Nicola.Tirelli@manchester.ac.uk (N.T.).
* E-mail: Marianne.Ashford@astrazeneca.com (M.A.).

* E-mail: kostas.kostarelos@manchester.ac.uk (K.K.).

ORCID ⊙

Kostas Kostarelos: 0000-0002-2224-6672

Author Contributions

Z.A. designed, planned, and led the study, preparing the L−AuNP hybrids and performing most of the biophysical characterization including quantification of the AuNPs using UV and ICP−MS measurements, anisotropy studies, purification, and separation studies, and prepared figures and wrote the manuscript. R.D. ran the MF system and prepared MF L−AuNP hybrids, optimized the parameters for MF experiments, performed the AFM data acquisition, analyzed and coordinated the cryo-TEM and CET imaging, and prepared Figures [5], and [7]. A.G performed and analyzed the C-FFF studies. E.P. acquired and analyzed STEM images. R.M. performed and analyzed the cryo-TEM images. A.M. acquired the TEM images. L.N. prepared samples for STEM imaging and provided advice on ICP−MS studies. M.J.L. performed and analyzed SANS studies. N.T. and K.K discussed the findings and reviewed the manuscript. Z.A., R.D., M.A., M.J.L, N.T., and K.K. discussed the findings, reviewed, and edited the manuscript.

Notes

The authors declare no competing financial interest.

■ REFERENCES

(1) Allen, T. M.; Cullis, P. R. Liposomal drug delivery systems: from concept to clinical applications. *Adv. Drug Delivery Rev.* **2013**, *65*, 36−48.

(2) Barenholz, Y. Doxil—The first FDA-approved nano-drug: Lessons learned. *J. Controlled Release* **2012**, *160*, 117−134.

(3) Li, X.; Hirsh, D. J..; Cabral-Lilly, D.; Zirkel, A.; Gruner, S. M.; Janoff, A. S.; Perkins, W. R. Doxorubicin physical state in solution and inside liposomes loaded via a pH gradient. *Biochim. Biophys. Acta, Biomembr.* **1998**, *1415*, 23−40.

(4) Lozano, N.; Al-Ahmady, Z. S.; Beziere, N. S.; Ntziachristos, V.; Kostarelos, K. Monoclonal antibody-targeted PEGylated liposome-ICG encapsulating doxorubicin as a potential theranostic agent. *Int. J. Pharm.* **2015**, *482*, 2−10.

(5) Chen, Y.; Bose, A.; Bothun, G. D. Controlled release from bilayer-decorated magnetoliposomes via electromagnetic heating. *ACS Nano* **2010**, *4*, 3215−3221.

(6) Koudelka, Š.; Turánek, J. Liposomal paclitaxel formulations. *J. Controlled Release* **2012**, *163*, 322−334.

(7) Sawant, R. R.; Torchilin, V. P. Challenges in development of targeted liposomal therapeutics. *AAPS J.* **2012**, *14*, 303−315.

(8) Gabizon, A.; Catane, R.; Uziely, B.; Kaufman, B.; Safra, T.; Cohen, R.; Martin, F.; Huang, A.; Barenholz, Y. Prolonged circulation time and enhanced accumulation in malignant exudates of doxorubicin encapsulated in polyethylene-glycol coated liposomes. *Cancer Res.* **1994**, *54*, 987−992.

(9) Gabizon, A.; Martin, F. Polyethylenglykol-umhülltes (pegy-liertes) liposomales Doxorubicin. *Drugs* **1997**, *54*, 15−21.

(10) Maestro, L. M.; Haro-González, P.; Sánchez-Iglesias, A.; Liz-Marzán, L. M.; García Solé, J.; Jaque, D. Quantum dot thermometry

evaluation of geometry dependent heating efficiency in gold nanoparticles. *Langmuir* **2014**, *30*, 1650−1658.

(11) Alkilany, A. M.; Thompson, L. B.; Boulos, S. P.; Sisco, P. N.; Murphy, C. J. Gold nanorods: their potential for photothermal therapeutics and drug delivery, tempered by the complexity of their biological interactions. *Adv. Drug Delivery Rev.* **2012**, *64*, 190−199.

(12) Jain, S.; Mishra, V.; Singh, P.; Dubey, P. K.; Saraf, D. K.; Vyas, S. P. RGD-anchored magnetic liposomes for monocytes/neutrophils-mediated brain targeting. *Int. J. Pharm.* **2003**, *261*, 43−55.

(13) Al-Jamal, W. T.; Al-Jamal, K. T.; Tian, B.; Lacerda, L.; Bornans, P. H.; Frederik, P. M.; Kostarelos, K. Lipid−Quantum Dot Bilayer Vesicles Enhance Tumor Cell Uptake and Retention in Vitro and in Vivo. *ACS Nano* **2008**, *2*, 408−418.

(14) Lozano, N.; Al-Jamal, W. T.; Taruttis, A.; Beziere, N.; Burton, N. C.; Van den Bossche, J.; Mazza, M.; Herzog, E.; Ntziachristos, V.; Kostarelos, K. Liposome-gold nanorod hybrids for high-resolution visualization deep in tissues. *J. Am. Chem. Soc.* **2012**, *134*, 13256−13258.

(15) Grzelczak, M.; Liz-Marzán, L. M. Colloidal nanoplasmonics: from building blocks to sensing devices. *Langmuir* **2013**, *29*, 4652−4663.

(16) Hormeño, S.; Gregorio-Godoy, P.; Pérez-Juste, J.; Liz-Marzán, L. M.; Juárez, B. H.; Arias-Gonzalez, J. R. Laser heating tunability by off-resonant irradiation of gold nanoparticles. *Small* **2014**, *10*, 376−384.

(17) Johannsen, M.; Thiesen, B.; Wust, P.; Jordan, A. Magnetic nanoparticle hyperthermia for prostate cancer. *Int. J. Hyperthermia* **2010**, *26*, 790−795.

(18) Visaria, R. K.; Griffin, R. J.; Williams, B. W.; Ebbini, E. S.; Paciotti, G. F.; Song, C. W.; Bischof, J. C. Enhancement of tumor thermal therapy using gold nanoparticle−assisted tumor necrosis factor-α delivery. *Mol. Cancer Ther.* **2006**, *5*, 1014−1020.

(19) Wong, K. K. Y.; Liu, X. Silver nanoparticles-the real "silver bullet" in clinical medicine? *MedChemComm* **2010**, *1*, 125−131.

(20) Liu, M.; Gan, L.; Chen, L.; Zhu, D.; Xu, Z.; Hao, Z.; Chen, L. A novel liposome-encapsulated hemoglobin/silica nanoparticle as an oxygen carrier. *Int. J. Pharm.* **2012**, *427*, 354−357.

(21) Lajunen, T.; Viitala, L.; Kontturi, L.-S.; Laaksonen, T.; Liang, H.; Vuorimaa-Laukkanen, E.; Viitala, T.; Le Guével, X.; Yliperttula, M.; Murtomäki, L.; Urtti, A. Light induced cytosolic drug delivery from liposomes with gold nanoparticles. *J. Controlled Release* **2015**, *203*, 85−98.

(22) Al-Ahmady, Z.; Kostarelos, K. Chemical Components for the Design of Temperature-Responsive Vesicles as Cancer Therapeutics. *Chem. Rev.* **2016**, *116*, 3883−3918.

(23) Preiss, M. R.; Bothun, G. D. Stimuli-responsive liposome-nanoparticle assemblies. *Expert Opin. Drug Delivery* **2011**, *8*, 1025−1040.

(24) Kojima, C.; Hirano, Y.; Yuba, E.; Harada, A.; Kono, K. Preparation and characterization of complexes of liposomes with gold nanoparticles. *Colloids Surf., B* **2008**, *66*, 246−252.

(25) Soga, K.; Tokuzen, K.; Tsuji, K.; Yamano, T.; Hyodo, H.; Kishimoto, H. NIR Bioimaging: Development of Liposome-Encapsulated, Rare-Earth-Doped Y2O3 Nanoparticles as Fluorescent Probes. *Eur. J. Inorg. Chem.* **2010**, *2010*, 2673−2677.

(26) Paasonen, L.; Sipilä, T.; Subrizi, A.; Laurinmäki, P.; Butcher, S. J.; Rappolt, M.; Yaghmur, A.; Urtti, A.; Yliperttula, M. Gold-embedded photosensitive liposomes for drug delivery: triggering mechanism and intracellular release. *J. Controlled Release* **2010**, *147*, 136−143.

(27) Tai, L.-A.; Tsai, P.-J.; Wang, Y.-C.; Wang, Y.-J.; Lo, L.-W.; Yang, C.-S. Thermosensitive liposomes entrapping iron oxide nanoparticles for controllable drug release. *Nanotechnology* **2009**, *20*, 135101.

(28) Wu, G.; Mikhailovsky, A.; Khant, H. A.; Fu, C.; Chiu, W.; Zasadzinski, J. A. Remotely triggered liposome release by near-infrared light absorption via hollow gold nanoshells. *J. Am. Chem. Soc.* **2008**, *130*, 8175−8177.

(29) Kastner, E.; Kaur, R.; Lowry, D.; Moghaddam, B.; Wilkinson, A.; Perrie, Y. High-throughput manufacturing of size-tuned liposomes by a new microfluidics method using enhanced statistical tools for characterization. *Int. J. Pharm.* **2014**, *477*, 361−368.

(30) Andar, A. U.; Hood, R. R.; Vreeland, W. N.; Devoe, D. L.; Swaan, P. W. Microfluidic preparation of liposomes to determine particle size influence on cellular uptake mechanisms. *Pharm. Res.* **2014**, *31*, 401−413.

(31) Leung, A. K. K.; Tam, Y. Y. C.; Chen, S.; Hafez, I. M.; Cullis, P. R. Microfluidic Mixing: A General Method for Encapsulating Macromolecules in Lipid Nanoparticle Systems. *J. Phys. Chem. B* **2015**, *119*, 8698−8706.

(32) Leung, A. K. K.; Tam, Y. Y. C.; Cullis, P. R. Lipid nanoparticles for short interfering RNA delivery. *Adv. Genet.* **2014**, *88*, 71−110.

(33) Walsh, C.; Ou, K.; Belliveau, N. M.; Leaver, T. J.; Wild, A. W.; Huft, J.; Lin, P. J.; Chen, S.; Leung, A. K.; Lee, J. B.; Hansen, C. L.; Taylor, R. J.; Ramsay, E. C.; Cullis, P. R. Microfluidic-based manufacture of siRNA-lipid nanoparticles for therapeutic applications. *Drug Delivery System*; Methods in Molecular Biology; Springer, 2014; Vol. *1141*, pp 109−120.

(34) Dong, Y.-D.; Tchung, E.; Nowell, C.; Kaga, S.; Leong, N.; Mehta, D.; Kaminskas, L. M.; Boyd, B. J. Microfluidic preparation of drug-loaded PEGylated liposomes, and the impact of liposome size on tumour retention and penetration. *J. Liposome Res.* **2017**, *29*, 1−9.

(35) Guimarães Sá Correia, M.; Briuglia, M. L.; Niosi, F.; Lamprou, D. A. Microfluidic manufacturing of phospholipid nanoparticles: Stability, encapsulation efficacy, and drug release. *Int. J. Pharm.* **2017**, *516*, 91−99.

(36) Joshi, S.; Hussain, M. T.; Roces, C. B.; Anderluzzi, G.; Kastner, E.; Salmaso, S.; Kirby, D. J.; Perrie, Y. Microfluidics based manufacture of liposomes simultaneously entrapping hydrophilic and lipophilic drugs. *Int. J. Pharm.* **2016**, *514*, 160−168.

(37) Yu, B.; Lee, R. J.; Lee, L. J. Microfluidic methods for production of liposomes. *Methods in Enzymology*; Academic Press, 2009; Vol. *465*, pp 129−141.

(38) Zhigaltsev, I. V.; Tam, Y. K.; Leung, A. K.; Cullis, P. R. Production of limit size nanoliposomal systems with potential utility as ultra-small drug delivery agents. *J. Liposome Res.* **2016**, *26*, 96−102.

(39) Hood, R. R.; Vreeland, W. N.; DeVoe, D. L. Microfluidic remote loading for rapid single-step liposomal drug preparation. *Lab Chip* **2014**, *14*, 3359−3367.

(40) Yu, B.; Zhu, J.; Xue, W.; Wu, Y.; Huang, X.; Lee, L. J.; Lee, R. J. Microfluidic assembly of lipid-based oligonucleotide nanoparticles. *Anticancer Res.* **2011**, *31*, 771−776.

(41) Balbino, T. A.; Serafin, J. M.; Radaic, A.; de Jesus, M. B.; de la Torre, L. G. Integrated microfluidic devices for the synthesis of nanoscale liposomes and lipoplexes. *Colloids Surf., B* **2017**, *152*, 406−413.

(42) Stewart, J. C. M. Colorimetric determination of phospholipids with ammonium ferrothiocyanate. *Anal. Biochem.* **1980**, *104*, 10−14.

(43) Al-Ahmady, Z.; Lozano, N.; Mei, K.-C.; Al-Jamal, W. T.; Kostarelos, K. Engineering thermosensitive liposome-nanoparticle hybrids loaded with doxorubicin for heat-triggered drug release. *Int. J. Pharm.* **2016**, *514*, 133−141.

(44) https://zenodo.org/record/583693#.WnHX-Khl_IU (access date March 2018).

(45) Kremer, J. R.; Mastronarde, D. N.; McIntosh, J. R. Computer visualization of three-dimensional image data using IMOD. *J. Struct. Biol.* **1996**, *116*, 71−76.

(46) Al-Ahmady, Z. S.; Al-Jamal, W. T.; Bossche, J. V.; Bui, T. T.; Drake, A. F.; Mason, A. J.; Kostarelos, K. Lipid-Peptide Vesicle Nanoscale Hybrids for Triggered Drug Release by Mild Hyperthermia in Vitro and in Vivo. *ACS Nano* **2012**, *6*, 9335−9346.

(47) Heenan, K. *The "FISH" Reference Manual (Data Fitting Program For Small-Angle Diffraction)*; Rutherford Appleton Laboratory, 1989, RAL Report 89-129 (Revised 2000).

(48) Carugo, D.; Bottaro, E.; Owen, J.; Stride, E.; Nastruzzi, C. Liposome production by microfluidics: potential and limiting factors. *Sci. Rep.* **2016**, *6*, 25876.

(49) Donno, R.; Gennari, A.; Lallana, E.; De La Rosa, J. M. R.; d'Arcy, R.; Treacher, K.; Hill, K.; Ashford, M.; Tirelli, N. Nanomanufacturing through microfluidic-assisted nanoprecipitation: Advanced analytics and structure-activity relationships. *Int. J. Pharm.* **2017**, *534*, 97−107.

(50) Maeki, M.; Fujishima, Y.; Sato, Y.; Yasui, T.; Kaji, N.; Ishida, A.; Tani, H.; Baba, Y.; Harashima, H.; Tokeshi, M. Understanding the formation mechanism of lipid nanoparticles in microfluidic devices with chaotic micromixers. *PLoS One* **2017**, *12*, No. e0187962.

(51) Patra, M.; Salonen, E.; Terama, E.; Vattulainen, I.; Faller, R.; Lee, B. W.; Holopainen, J.; Karttunen, M. Under the Influence of Alcohol: The Effect of Ethanol and Methanol on Lipid Bilayers. *Biophys. J.* **2006**, *90*, 1121−1135.

(52) Joshi, S.; Hussain, M. T.; Roces, C. B.; Anderluzzi, G.; Kastner, E.; Salmaso, S.; Kirby, D. J.; Perrie, Y. Microfluidics based manufacture of liposomes simultaneously entrapping hydrophilic and lipophilic drugs. *Int. J. Pharm.* **2016**, *514*, 160−168.

(53) Ali, M. H.; Moghaddam, B.; Kirby, D. J.; Mohammed, A. R.; Perrie, Y. The role of lipid geometry in designing liposomes for the solubilisation of poorly water soluble drugs. *Int. J. Pharm.* **2013**, *453*, 225−232.

(54) Ali, M. H.; Kirby, D. J.; Mohammed, A. R.; Perrie, Y. Solubilisation of drugs within liposomal bilayers: alternatives to cholesterol as a membrane stabilising agent. *J. Pharm. Pharmacol.* **2010**, *62*, 1646−1655.

(55) Mohammed, A. R.; Weston, N.; Coombes, A. G. A.; Fitzgerald, M.; Perrie, Y. Liposome formulation of poorly water soluble drugs: optimisation of drug loading and ESEM analysis of stability. *Int. J. Pharm.* **2004**, *285*, 23−34.

(56) Jahn, A.; Stavis, S. M.; Hong, J. S.; Vreeland, W. N.; DeVoe, D. L.; Gaitan, M. Microfluidic mixing and the formation of nanoscale lipid vesicles. *ACS Nano* **2010**, *4*, 2077−2087.

(57) Jahn, A.; Vreeland, W. N.; DeVoe, D. L.; Locascio, L. E.; Gaitan, M. Microfluidic directed formation of liposomes of controlled size. *Langmuir* **2007**, *23*, 6289−6293.

(58) Garbuzenko, O.; Barenholz, Y.; Priev, A. Effect of grafted PEG on liposome size and on compressibility and packing of lipid bilayer. *Chem. Phys. Lipids* **2005**, *135*, 117−129.

(59) Kitayama, H.; Takechi, Y.; Tamai, N.; Matsuki, H.; Yomota, C.; Saito, H. Thermotropic phase behavior of hydrogenated soybean phosphatidylcholine-cholesterol binary liposome membrane. *Chem. Pharm. Bull.* **2014**, *62*, 58−63.

(60) Szoka, F., Jr.; Papahadjopoulos, D. Procedure for preparation of liposomes with large internal aqueous space and high capture by reverse-phase evaporation. *Proc. Natl. Acad. Sci. U.S.A.* **1978**, *75*, 4194−4198.

(61) Reiner, J. E.; Jahn, A.; Stavis, S. M.; Culbertson, M. J.; Vreeland, W. N.; Burden, D. L.; Geist, J.; Gaitan, M. Accurate optical analysis of single-molecule entrapment in nanoscale vesicles. *Anal. Chem.* **2010**, *82*, 180−188.

(62) Lee, J.-H.; Shin, Y.; Lee, W.; Whang, K.; Kim, D.; Lee, L. P.; Choi, J. W.; Kang, T. General and programmable synthesis of hybrid liposome/metal nanoparticles. *Sci. Adv.* **2016**, *2*, No. e1601838.

(63) Park, S.-H.; Oh, S.-G.; Mun, J.-Y.; Han, S.-S. Effects of silver nanoparticles on the fluidity of bilayer in phospholipid liposome. *Colloids Surf., B* **2005**, *44*, 117−122.

(64) Park, S.-H.; Oh, S.-G.; Mun, J.-Y.; Han, S.-S. Loading of gold nanoparticles inside the DPPC bilayers of liposome and their effects on membrane fluidities. *Colloids Surf., B* **2006**, *48*, 112−118.

(65) Park, S.-H.; Oh, S.-G.; Suh, K.-D.; Han, S.-H.; Chung, D. J.; Mun, J.-Y.; Han, S.-S.; Kim, J.-W. Control over micro-fluidity of liposomal membranes by hybridizing metal nanoparticles. *Colloids Surf., B* **2009**, *70*, 108−113.

(66) Haynes, D. H.; Simkowitz, P. 1-Anilino-8-naphthalenesulfonate: a fluorescent probe of ion and ionophore transport kinetics and trans-membrane asymmetry. *J. Membr. Biol.* **1977**, *33*, 63−108.

(67) Slavík, J. Anilinonaphthalene sulfonate as a probe of membrane composition and function. *Biochim. Biophys. Acta* **1982**, *694*, 1−25.

(68) Bothun, G. D. Hydrophobic silver nanoparticles trapped in lipid bilayers: Size distribution, bilayer phase behavior, and optical properties. *J. Nanobiotechnol.* **2008**, *6*, 13.

(69) Tian, B.; Al-Jamal, W. T.; Al-Jamal, K. T.; Kostarelos, K. Doxorubicin-loaded lipid-quantum dot hybrids: Surface topography and release properties. *Int. J. Pharm.* **2011**, *416*, 443−447.